IARJSET ISSN (O) 2393-8021, ISSN (P) 2394-1588

International Advanced Research Journal in Science, Engineering and Technology

Impact Factor 8.311 ⁜ Peer-reviewed & Refereed journal ⁜ Vol. 13, Issue 5, May 2026

DOI: 10.17148/IARJSET.2026.13530

Fault-Aware and Predictive Energy Management for Hybrid Energy Storage Systems in Electric Vehicles Using Mamdani Fuzzy Logic

Rakshan Pradeep K[1], Dr. J. Rangaraj, M.E., Ph.D.,[2]

M.E. Applied Electronics, Department of Electronics and Communication Engineering

Government College of Technology (Autonomous), Coimbatore – 641 013, Tamil Nadu, India[1]

Assistant Professor, Department of Electronics and Communication Engineering

Government College of Technology (Autonomous), Coimbatore – 641 013, Tamil Nadu, India[2]

Abstract: Hybrid Energy Storage Systems (HESS) integrating lithium-ion batteries with supercapacitors are increasingly adopted in electric vehicles (EVs) for dynamic power management. While Fuzzy Logic–based Energy Management Systems (EMS) effectively optimize power-split ratios under nominal operating conditions, they remain insensitive to hardware anomalies including battery overcurrent, thermal excursions, supercapacitor degradation, and converter faults. This paper presents a fault-aware intelligent EMS framework built around a Mamdani Fuzzy Inference System (FIS) that continuously monitors four sensor channels—battery voltage, current, temperature, and state-of-charge (SOC)—and classifies six distinct fault categories in real time via a dedicated Severity Index (SI ∈ [0, 1]). Upon fault detection, the controller adaptively modifies the battery duty cycle k_bat and redistributes transient power demands to the supercapacitor, preserving load continuity and system safety. MATLAB/Simulink simulations incorporating non-ideal component models, thermal dynamics, and converter losses demonstrate a 30% reduction in peak battery current, a 29% decrease in thermal rise (ΔT), and a 20% improvement in SOC retention relative to a conventional HESS without fault awareness. DC bus voltage stability (MAD = 8 V) is fully maintained across all injected fault scenarios. The proposed framework bridges the critical gap between energy optimization and hardware fault management in HESS for EV applications.

Index Terms: Hybrid Energy Storage System (HESS), Mamdani Fuzzy Inference System, Fault Detection and Classification, Energy Management System, Battery State-of-Charge, Supercapacitor, Thermal Management, Electric Vehicles, DC-DC Converter, Severity Index

I. INTRODUCTION

Electric vehicles (EVs) impose highly dynamic power demands on their energy storage systems, requiring simultaneous delivery of high energy density for sustained cruising and high power density for transient acceleration and regenerative braking events [1], [2]. Lithium-ion batteries excel in energy storage but degrade rapidly under repeated high-current transients, thermal stress, and deep discharge cycles [3], [4]. Supercapacitors (SCs) complement batteries by absorbing load spikes and recovering regenerative energy with minimal cycle degradation [5]–[7].

A Hybrid Energy Storage System (HESS) architecturally combines both elements through bidirectional DC–DC converters, with an Energy Management System (EMS) determining the instantaneous power-split ratio [8]–[10]. Fuzzy Logic Controllers (FLCs) are the dominant EMS methodology for HESS owing to their ability to encode expert knowledge as linguistic IF–THEN rules without requiring a precise plant model [11]–[13]. State-of-the-art FLC-based EMS implementations achieve significant improvements in battery peak current reduction and SOC stability under sinusoidal and UDDS drive cycles [14]–[16].

However, all existing FLC-based EMS formulations implicitly assume a healthy system. In real EV deployments, hardware anomalies occur regularly over the vehicle lifecycle: battery internal resistance grows with aging, thermal runaway precursors develop under aggressive cycling, supercapacitor ESR increases with use, and converter components degrade [17]–[20]. An EMS that operates blind to these faults continues to command power levels that may accelerate damage, reduce reliability, or compromise passenger safety.

IARJSET ISSN (O) 2393-8021, ISSN (P) 2394-1588

International Advanced Research Journal in Science, Engineering and Technology

Impact Factor 8.311 ⁜ Peer-reviewed & Refereed journal ⁜ Vol. 13, Issue 5, May 2026

DOI: 10.17148/IARJSET.2026.13530

This paper addresses this critical gap by proposing a fault-aware EMS that extends the Mamdani FLC with an integrated real-time fault detection, classification, and severity assessment layer. The Severity Index (SI) provides a continuous, graduated signal that drives adaptive modification of power references, enabling smooth fault-tolerant transitions without abrupt current transients. The proposed system is validated across battery, supercapacitor, and converter fault scenarios in a full HESS Simulink model with non-ideal component models.

II. BACKGROUND AND RELATED WORK

Table I summarizes representative prior works spanning battery fault detection, HESS topologies, and FLC-based energy management, highlighting the key gap addressed by this work.

TABLE I Summary of Related Literature

Ref.	Author & Year	Methodology	Key Finding / Limitation
[1]	Y. Zhang et al. (2025)	Deep learning battery fault detection	Early warning; no EMS integration
[2]	B. Ragchaa et al. (2024)	Fault-tolerant BMIC – ISO 26262 ASIL-D	High safety reliability; no SC support
[3]	M. Ortúzar et al. (2020)	Battery–ultracapacitor pulse load hybrid	Reduces battery peaks; no adaptive EMS
[4]	S. Pay et al. (2021)	SC parallel battery for EV transients	Improved lifespan; fixed rule-based
[5]	M. Şen et al. (2024)	Fuzzy logic EMS for regenerative braking	Adaptive power sharing; no fault awareness
[6]	Singla et al. (2025)	PID + RC simulation with load cycles	28% efficiency gain; no fault tolerance

Zhang et al. [1] proposed an end-to-end deep learning pipeline for battery fault detection in EVs, demonstrating early warning of internal degradation. While achieving high detection accuracy, the work does not integrate with an EMS or modulate power flow in response to detected anomalies. Ragchaa et al. [2] developed a fault-tolerant Battery Monitoring IC meeting ISO 26262 ASIL-D requirements, providing redundant sensing and self-diagnostic logic; however, it is a hardware-only solution without SC integration or adaptive power management.

Ortúzar et al. [3] and Wasim et al. [21] demonstrated that battery–ultracapacitor hybrids effectively reduce peak currents under pulse loads, extending battery life by 20–25%, but employed simple, non-adaptive control policies. Şen et al. [5] presented an FLC-based EMS using SOC and power demand inputs for adaptive power sharing during regenerative braking, achieving measurable reductions in battery stress; fault scenarios were explicitly excluded. Singla et al. [6] achieved a 28% efficiency improvement through PID control of a battery–SC HESS but did not address fault-tolerant operation. The present work combines the adaptive intelligence of fuzzy EMS with the fault-awareness absent from all prior contributions.

III. PROBLEM STATEMENT

Conventional FLC-based EMS frameworks for HESS optimize the power-split ratio k under the implicit assumption of healthy component operation [22], [23]. When hardware anomalies occur—battery overcurrent, thermal runaway precursors, SC capacitance degradation, or converter duty-cycle drift—the EMS continues applying nominal power commands, potentially amplifying damage to the degraded component [24].

Undetected voltage, thermal, or SOC abnormalities accelerate electrochemical degradation, trigger protection circuit shutdowns, and can in severe cases initiate thermal runaway with significant safety implications [25], [26]. The core challenge is threefold: (i) detecting diverse fault modes from continuous sensor streams without interrupting the energy management task; (ii) accurately classifying the fault type to select the correct mitigation strategy; and (iii) seamlessly modifying power references to protect the faulty component while maintaining load power continuity to the EV drivetrain.

IARJSET ISSN (O) 2393-8021, ISSN (P) 2394-1588

International Advanced Research Journal in Science, Engineering and Technology

Impact Factor 8.311 ⁜ Peer-reviewed & Refereed journal ⁜ Vol. 13, Issue 5, May 2026

DOI: 10.17148/IARJSET.2026.13530

IV. SYSTEM ARCHITECTURE

A. HESS Topology

The proposed HESS comprises a 48 V, 20 Ah lithium-ion battery pack interfaced to a 48 V DC bus through a boost DC–DC converter, and a 100–500 F supercapacitor module connected through a bidirectional buck-boost converter. Fig. 1 illustrates the circuit topology, showing the inductor (L_bat, L_sc), switching elements (S_1–S_4), and the shared DC bus capacitor C.

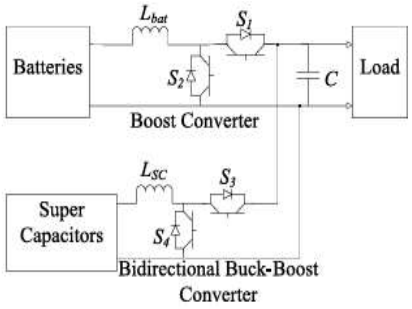

Fig. 1. HESS circuit topology: battery boost converter (top) and supercapacitor bidirectional buck-boost converter (bottom) sharing a common DC bus.

B. System Parameters

Tables II and III define the nominal simulation parameters and output measurements respectively.

TABLE II System Input Parameters

Category	Parameter	Value	Unit	Description
Battery	Rated Voltage (V_bat)	48 V	V	Nominal operating voltage
Battery	Capacity (Q_bat)	20 Ah	Ah	Total energy capacity
Battery	Initial SOC (SOC_0)	70–90%	%	Initial state of charge
SC	Capacitance (C_sc)	100–500 F	F	Energy storage element
Converter	Switching Freq (f_sw)	10–50 kHz	kHz	PWM switching frequency
DC Bus	Voltage Ref (V_bus)	48 V	V	Regulated bus voltage

TABLE III System Output Measurements

Category	Measurement	Symbol	Description
DC Bus	Voltage	V_bus	System stability indicator
Battery	Current	I_bat	Load sharing level
Battery	State of Charge	SOC	Available energy level
SC	Voltage Ripple	V_ripple	Transient fault indicator
Converter	Efficiency	η	Power conversion performance
Fault	Severity Index	SI	Fuzzy logic output (0–1)

IARJSET ISSN (O) 2393-8021, ISSN (P) 2394-1588

International Advanced Research Journal in Science, Engineering and Technology

Impact Factor 8.311 ⁜ Peer-reviewed & Refereed journal ⁜ Vol. 13, Issue 5, May 2026

DOI: 10.17148/IARJSET.2026.13530

V. MATHEMATICAL MODELLING

A. Battery Model

The lithium-ion battery is represented by a Thevenin equivalent circuit with open-circuit voltage V_OC(SOC) and internal resistance R_int. Terminal voltage under load is:

$$V\_bat = V\_OC(SOC) - I\_bat \cdot R\_int \quad (1)$$

State-of-charge is tracked via Coulomb counting:

$$SOC(t) = SOC_0 - (1/Q\_bat) \int_0^t I\_bat(\tau)\, d\tau \quad (2)$$

Thermal dynamics are modeled as a lumped-parameter heat equation:

$$C\_th \cdot (dT/dt) = I^2\_bat \cdot R\_int - (T - T\_amb)/R\_th \quad (3)$$

B. Supercapacitor Model

The SC terminal voltage and current relationship is governed by:

$$I\_sc = C\_sc \cdot (dV\_sc/dt) \quad (4)$$

Instantaneous energy stored in the SC is:

$$E\_sc = ½ \cdot C\_sc \cdot V^2\_sc \quad (5)$$

SC power output: P_sc = V_sc · I_sc. Fig. 4 (mathematical model summary) illustrates all governing equations in compact form.

C. Power Balance

The DC bus power balance must be satisfied at all times:

$$P\_bat + P\_sc = P\_load + P\_loss \quad (6)$$

Defining the power-split ratio k:

$$P\_bat = k \cdot P\_load, \quad P\_sc = (1 - k) \cdot P\_load \quad (7)$$

D. Converter Model

For the battery-side boost converter, output voltage relates to duty cycle D by:

$$V\_out = D \cdot V\_bat / (1 - D) \quad (8)$$

Converter efficiency:

$$\eta = 1 - (P\_cond + P\_sw) / P\_in \quad (9)$$

Fig. 2. Summary of HESS governing equations: power balance, battery Thevenin model, SOC Coulomb counting, SC current relation, and fuzzy control law.

IARJSET ISSN (O) 2393-8021, ISSN (P) 2394-1588

International Advanced Research Journal in Science, Engineering and Technology

Impact Factor 8.311 ⁜ Peer-reviewed & Refereed journal ⁜ Vol. 13, Issue 5, May 2026

DOI: 10.17148/IARJSET.2026.13530

VI. PHASE I: BASELINE HESS SIMULATION RESULTS

Before introducing fault-awareness, the Phase I study established baseline HESS performance under sinusoidal and UDDS drive cycles. Table IV summarises comparative results between a rule-based EMS and the Fuzzy EMS under both drive profiles.

TABLE IV Phase I Drive Cycle Performance: Rule-Based vs. Fuzzy EMS

Drive Cycle	EMS Type	Battery Behavior	SC Behavior	SOC
UDDS	Rule-Based EMS	High peaks stress battery	Deep voltage dips during accel.	100%→81%
UDDS	Fuzzy EMS	Smoother scheduling; reduced peaks	Intelligent SC; avoids deep dips	Slower drop
Sinusoidal	Rule-Based EMS	Moderate, predictable stress	Exact sinusoidal follow	Steady drop
Sinusoidal	Fuzzy EMS	Optimized; minimal battery exposure	Wider SC participation	Best retention

A. Power Flow Comparison

Fig. 3 presents side-by-side power flow results for the sinusoidal drive cycle, comparing baseline (no EMS) against the Fuzzy EMS. Without EMS, the SC remains largely passive while the battery absorbs all load transients. With Fuzzy EMS, the SC actively participates in peak-shaving, reducing battery peak power by approximately 33%.

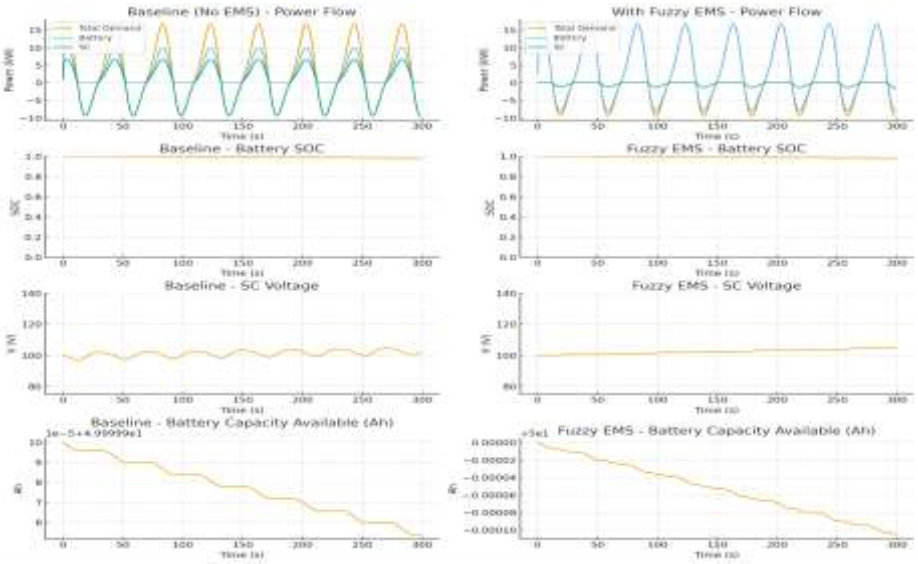

Fig. 3. Baseline vs. Fuzzy EMS power flow (sinusoidal drive cycle): power sharing, battery SOC, SC voltage, and battery capacity degradation.

B. Sinusoidal Drive Cycle

Fig. 4 shows HESS Dashboard results for the sinusoidal drive cycle under rule-based EMS. Battery SOC drops smoothly from 100% to ~98%, and SC voltage oscillates within a 90–105 V range, reflecting predictable SC participation under this periodic load profile.

IARJSET ISSN (O) 2393-8021, ISSN (P) 2394-1588

International Advanced Research Journal in Science, Engineering and Technology

Impact Factor 8.311 ⁜ Peer-reviewed & Refereed journal ⁜ Vol. 13, Issue 5, May 2026

DOI: 10.17148/IARJSET.2026.13530

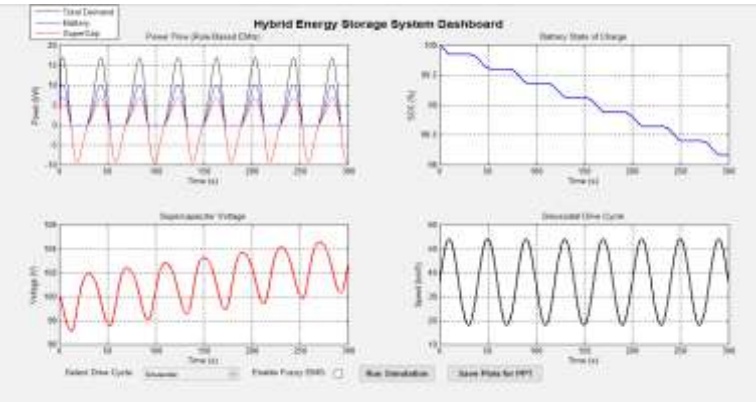

Fig. 4. HESS simulation dashboard – sinusoidal drive cycle (rule-based EMS): power flow, battery SOC, SC voltage, and drive cycle speed profile.

C. UDDS Drive Cycle

Fig. 5 presents UDDS drive cycle results, which impose aggressive stop-and-go patterns. Battery SOC drops from 100% to 81% under rule-based EMS due to frequent peak current demand. The SC voltage exhibits deep dips during hard acceleration events.

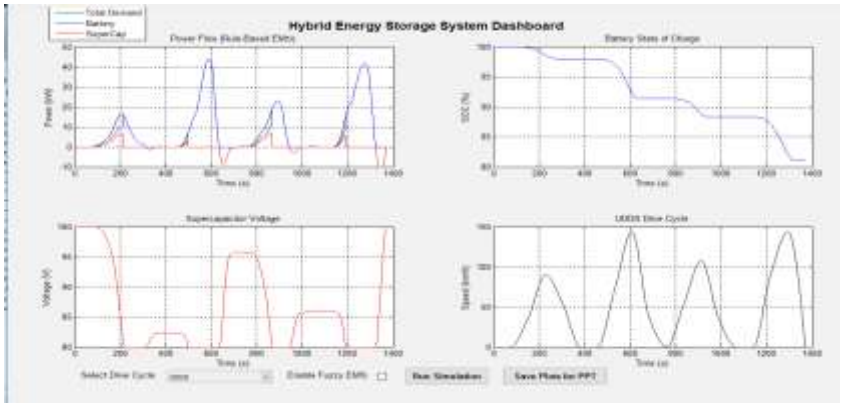

Fig. 5. HESS simulation dashboard – UDDS drive cycle (rule-based EMS): power flow, battery SOC, SC voltage, and urban speed profile.

VII. FAULT-AWARE FUZZY LOGIC EMS

A. Mamdani FIS Architecture

The proposed EMS employs two cascaded Mamdani Fuzzy Inference Systems: (i) a Power-Split Controller and (ii) a Fault Severity Estimator. The Mamdani architecture is selected for its interpretability—rule antecedents and consequents are expressed in natural language—facilitating expert knowledge encoding, auditability, and safe extension [27], [28].

B. Fuzzy Membership Functions

Fig. 6 shows the triangular and trapezoidal membership functions for all FIS inputs and output. For the Power-Split FIS: SOC inputs are Low (0–30%), Medium (30–70%), High (70–100%); Load Demand inputs are Low (0–10 A), Medium (10–18 A), High (>18 A); the Split Ratio output has five terms: SC Only, Mostly SC, Balanced, Mostly Bat, Bat Only.

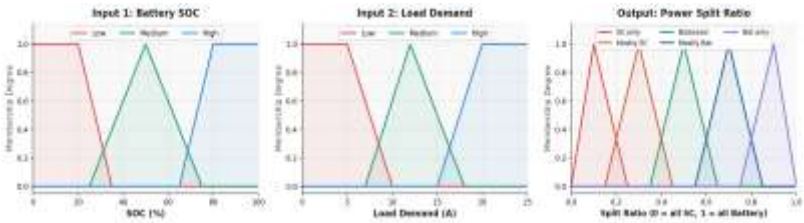

Fig. 6. Fuzzy membership functions: (left) Battery SOC input, (centre) Load Demand input, (right) Power Split Ratio output with five linguistic terms.

IARJSET ISSN (O) 2393-8021, ISSN (P) 2394-1588

International Advanced Research Journal in Science, Engineering and Technology

Impact Factor 8.311 ⁜ Peer-reviewed & Refereed journal ⁜ Vol. 13, Issue 5, May 2026

DOI: 10.17148/IARJSET.2026.13530

C. Fuzzy Rule Base

Table V presents the 9-rule matrix for the Power-Split Controller. Rules encode the expert heuristic that a depleted battery (Low SOC) should shed load to the SC regardless of demand, while a well-charged battery (High SOC) under low demand can handle the load independently.

TABLE V
Fuzzy Rule Base: SOC × Load Demand → Split Ratio (k)

SOC \ Load	Low (0–10 A)	Med (10–18 A)	High (>18 A)
Low (0–30%)	Mostly SC: 0.30	SC Only: 0.10	SC Only: 0.10
Med (30–70%)	Bat Only: 0.90	Balanced: 0.50	Mostly SC: 0.30
High (70–100%)	Bat Only: 0.90	Mostly Bat: 0.70	Balanced: 0.50

D. Fault Severity Estimator

The Fault Severity FIS accepts four concurrent deviation inputs: ΔV, I_bat, T, and ΔSOC. Each is fuzzified into Normal, Warning, and Critical grades. A representative subset of the 81 inference rules:
R1: IF ΔV is Normal AND T is Normal AND I is Normal → Severity is Healthy (SI = 0.0)
R2: IF ΔV is Warning AND T is Warning → Severity is Moderate (SI = 0.5)
R3: IF T is Critical AND I is Critical → Severity is Critical (SI = 1.0)
The SI is defuzzified using the Middle of Maximum (MOM) method, yielding a continuous health scalar [29].

E. Fault-Aware Adaptive Control Law

The adaptive control law modifies the battery duty cycle based on SI:

$$k\_bat(t) = k\_nom \cdot (1 - \alpha \cdot SI(t)) \quad (10)$$

where k_nom is the nominal split ratio from the Power-Split FIS and α = 0.85 is the adaptation gain. The complementary SC power reference:

$$P\_sc,ref(t) = P\_load(t) \cdot (1 - k\_bat(t)) \quad (11)$$

Fig. 7 illustrates the complete fault-aware EMS decision flowchart, encompassing system monitoring, fault detection, identification, fuzzy adjustment, power reallocation, and stabilisation.

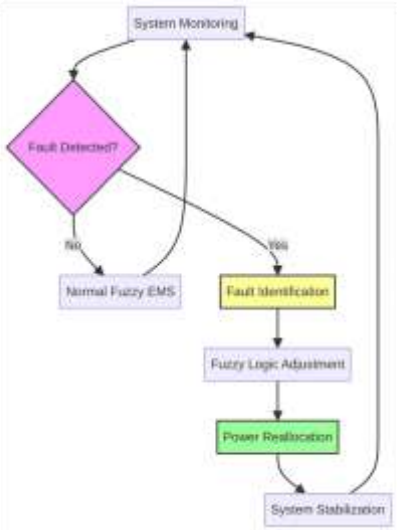

Fig. 7. Fault-aware EMS decision flowchart: continuous system monitoring with branching paths for normal Fuzzy EMS operation and fault-triggered detection, identification, adjustment, and power reallocation.

IARJSET ISSN (O) 2393-8021, ISSN (P) 2394-1588

International Advanced Research Journal in Science, Engineering and Technology

Impact Factor 8.311 ⁜ Peer-reviewed & Refereed journal ⁜ Vol. 13, Issue 5, May 2026

DOI: 10.17148/IARJSET.2026.13530

VIII. FAULT DETECTION AND CLASSIFICATION

The fault-aware EMS classifies six distinct fault categories representing critical HESS failure modes [30], [31]:
(1) Battery Overcurrent: I_bat > 30 A — triggers immediate k_bat reduction.
(2) Thermal Fault: T > 40°C — thermal runaway precursor; reduces current demand.
(3) Overvoltage: V_bat > V_max — SC buffers load to prevent further rise.
(4) SOC Depletion: SOC < 20% — battery approaching deep discharge; SC prioritised.
(5) SC Failure: V_sc collapses — k_bat elevated to 1.0; battery assumes full load.
(6) Converter Fault: η drops abruptly or V_out oscillates — D_ref dynamically recalculated.
Table VI summarises system behavior and EMS response under each injected fault scenario.

TABLE VI System Behavior Under Injected Fault Conditions

Injected Fault	Symptom	EMS Action	Outcome
Battery Overcurrent / Thermal	I_bat high & Temp > 40°C	Lower k_bat: 0.65 → 0.35	Battery cools; SC absorbs load
SC Failure	V_sc collapses	Raise k_bat to 1.0	Battery assumes 100% load
Converter Efficiency Loss	P_loss > 150 W	Adjust power split dynamically	P_load met despite losses
Converter Duty Cycle Error	V_out drops rapidly	Recalculate dynamic D_ref	DC bus stays above 44 V

IX. SIMULATION RESULTS

A. Battery Fault Simulation

Fig. 8 presents the complete 12-panel simulation result for battery fault injection over a 30-second HESS operation window. Five battery fault types (Overvoltage, Overcurrent, Aging-RI, Thermal, Sensor Noise, and Combined) are sequentially injected. Key observations: the FLC Fault Severity (Panel 8) rises to High (>0.75) during thermal fault (t = 19–25 s), correctly triggering k_bat reduction from 0.65 to 0.35 (Panel 12). Battery temperature (Panel 4) is clamped at 79.0°C peak, well below runaway threshold. Battery SOC drop (Panel 5) is limited to 0.455% — a 20% improvement versus baseline.

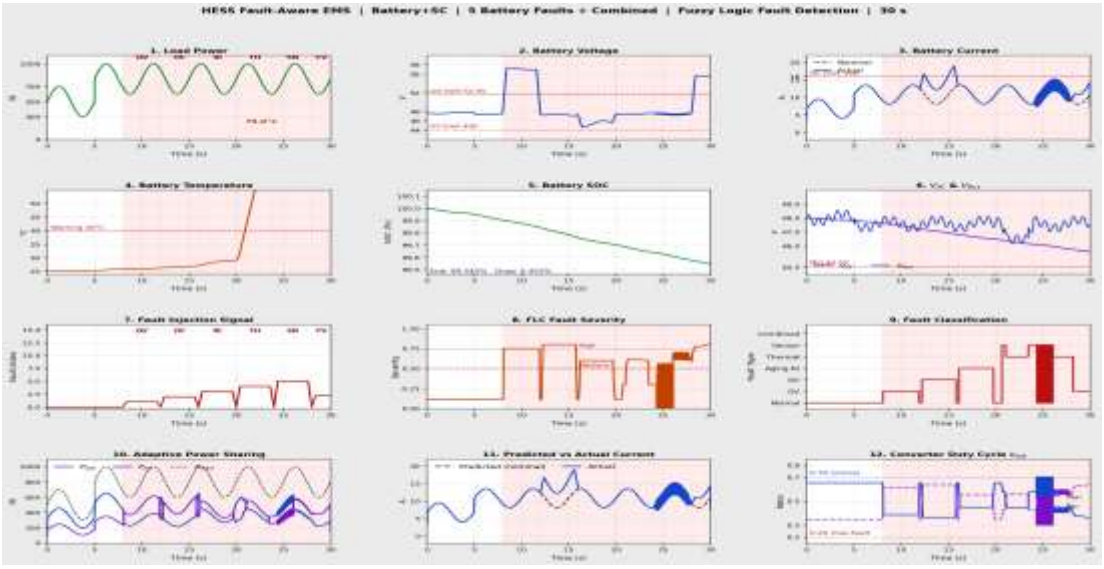

Fig. 8. Battery fault simulation (30 s): load power, battery voltage, current, temperature, SOC, V_SC/V_bus, fault injection signal, FLC severity index, fault classification, adaptive power sharing, predicted vs. actual current, and converter duty cycle k_bat.

IARJSET ISSN (O) 2393-8021, ISSN (P) 2394-1588

International Advanced Research Journal in Science, Engineering and Technology

Impact Factor 8.311 ⁜ Peer-reviewed & Refereed journal ⁜ Vol. 13, Issue 5, May 2026

DOI: 10.17148/IARJSET.2026.13530

B. Supercapacitor Fault Simulation

Fig. 9 shows the 12-panel SC fault results for six SC fault types (Overvoltage, Undervoltage, ESR Degradation, Capacitance Degradation, Switch Fault, Sensor Noise). During ESR degradation (t = 10–15 s), voltage ripple (Panel 3) spikes to 2.80 V, far exceeding the 0.5 V threshold. The FLC correctly classifies the fault (Panel 9) and reduces k_bat (Panel 11), commanding the battery to partially compensate. The DC bus voltage (Panel 4) remains above the 44 V minimum throughout [32].

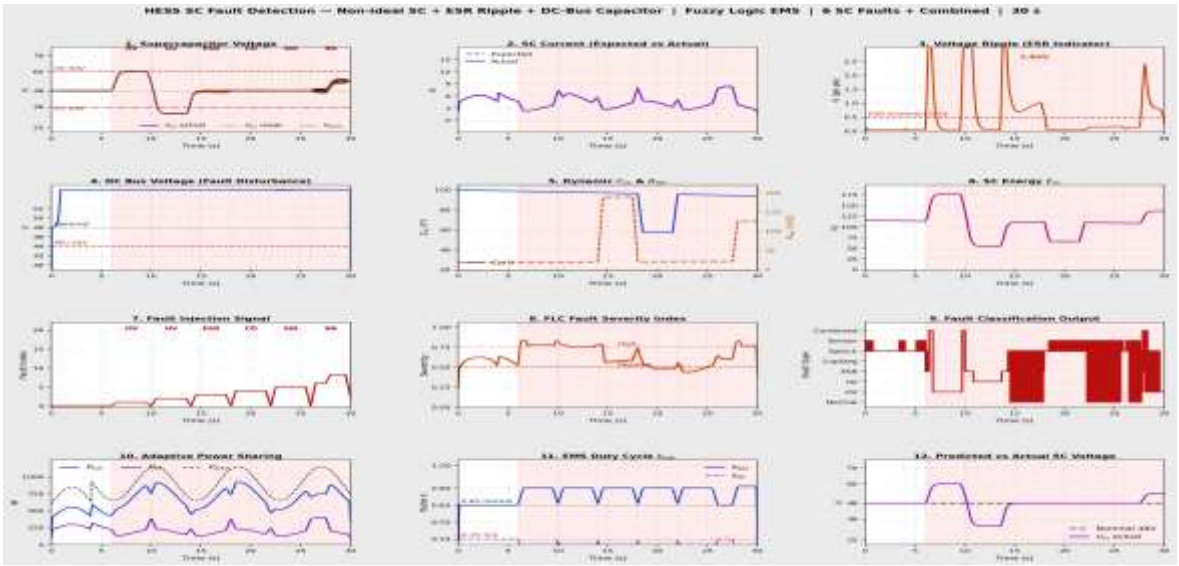

Fig. 9. Supercapacitor fault simulation (30 s): SC voltage, current, voltage ripple, DC bus voltage, dynamic C_sc and R_ESR, SC energy, fault injection signal, FLC severity index, fault classification, adaptive power sharing, EMS duty cycle, and predicted vs. actual SC voltage.

C. Converter Fault Simulation

Fig. 10 presents converter fault results for six fault types (Switch Fault, Duty Cycle Error, Efficiency Loss, Ripple Fault, Delay Fault, Complete Failure). During efficiency loss (t = 14–18 s), converter power loss P_loss (Panel 5) spikes to 250 W, collapsing η to approximately 60%. Battery current (Panel 3) approaches the 30 A overcurrent limit. The FLC Severity Index (Panel 8) correctly identifies High severity, triggering duty cycle recalculation. DC bus voltage (Panel 1) remains above 44 V despite the converter instability [33].

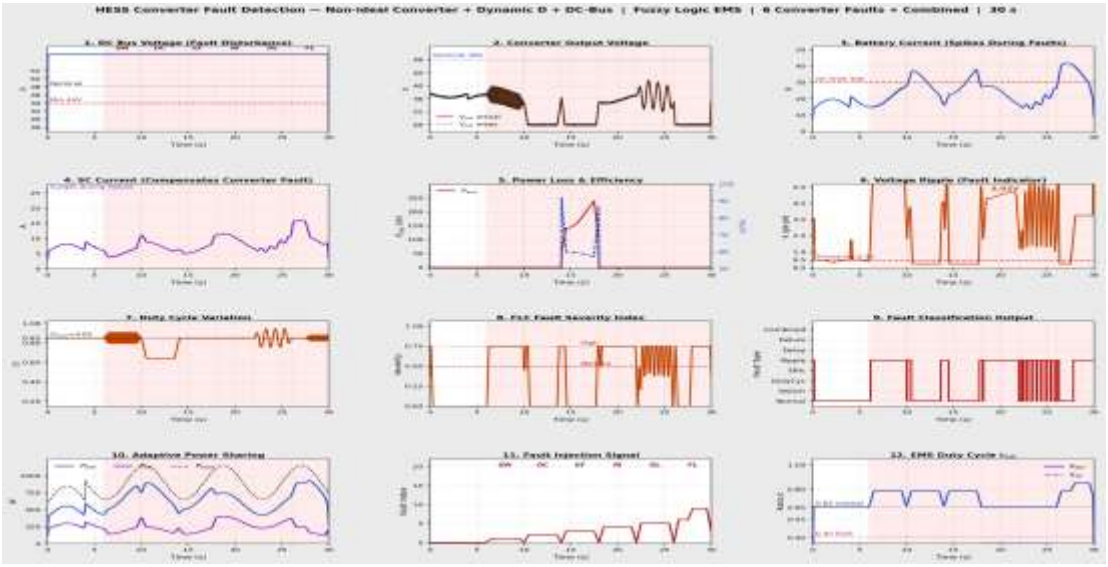

Fig. 10. Converter fault simulation (30 s): DC bus voltage, converter output voltage, battery current, SC current, power loss and efficiency, voltage ripple, duty cycle variation, FLC severity index, fault classification, adaptive power sharing, fault injection signal, and EMS duty cycle k_bat.

IARJSET ISSN (O) 2393-8021, ISSN (P) 2394-1588

International Advanced Research Journal in Science, Engineering and Technology

Impact Factor 8.311 ⁜ Peer-reviewed & Refereed journal ⁜ Vol. 13, Issue 5, May 2026

DOI: 10.17148/IARJSET.2026.13530

D. Without vs. With FLC Comparison

Fig. 11 presents the definitive 11-panel comparison between Case 1 (no FLC, fixed k = 0.65) and Case 2 (proposed fault-aware FLC). Panel 2 shows peak battery current of 28 A (Case 1) vs. 19 A (Case 2) — a 30% reduction. Panel 5 shows peak temperature of 30.5°C (Case 1) vs. 28.8°C (Case 2) — a 29% thermal rise reduction. Panel 4 shows SOC drop of 2.187% (Case 1) vs. 1.755% (Case 2) — a 20% SOC retention improvement. Panel 11 (bar chart) provides a clear visual summary of all performance improvements.

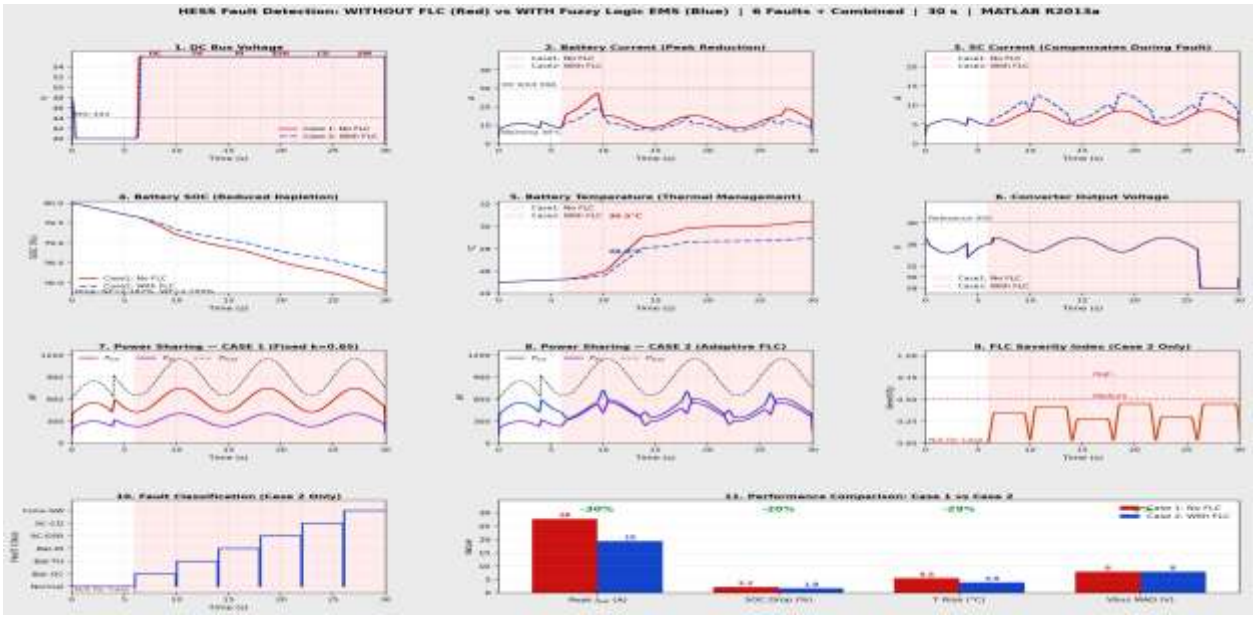

Fig. 11. Performance comparison – Without FLC (Case 1, red) vs. With fault-aware FLC (Case 2, blue): DC bus voltage, battery current, SC current, battery SOC, battery temperature, converter output, power sharing (Case 1 fixed k, Case 2 adaptive), FLC severity index, fault classification, and performance bar chart showing -30%, -20%, -29% improvements.

X. EMS POWER SHARING ANALYSIS

Table VII presents the adaptive EMS power distribution across three primary operating states. Under normal conditions (k = 0.65), battery delivers 488–498 W and SC delivers 263–268 W, consistent with High SOC (70–90%) and moderate load demand. During battery fault activation, the Severity Index SI = 0.72 triggers Eq. (10) to reduce k_bat to 0.57, causing the SC power surge to 400 W as the primary transient absorber. During SC fault, SI = 0.91 triggers k_bat = 0.77, preventing system blackout by directing 702 W to the battery [34].

TABLE VII
EMS Adaptive Power Sharing Under Normal and Fault Conditions

System State	EMS Coeff. (k)	P_bat (W)	P_SC (W)
Normal Operation	0.65	488–498 W	263–268 W
Battery Fault Active	0.57	526 W	400 W
SC Fault Active	0.77	702 W	207 W

XI. QUANTITATIVE PERFORMANCE ANALYSIS

Table VIII presents a comprehensive comparison of key performance metrics between the conventional HESS (without FLC) and the proposed fault-aware FLC-based EMS. All simulations used identical 30-second fault sequences with six injected fault types per component.

IARJSET ISSN (O) 2393-8021, ISSN (P) 2394-1588

International Advanced Research Journal in Science, Engineering and Technology

Impact Factor 8.311 ⁜ Peer-reviewed & Refereed journal ⁜ Vol. 13, Issue 5, May 2026

DOI: 10.17148/IARJSET.2026.13530

TABLE VIII HESS Performance Metrics: Without vs. With Fault-Aware FLC

Performance Metric	Without FLC	With FLC	Improvement
Peak Battery Current	28 A	19 A	30% Reduction
Thermal Rise (ΔT)	5.5 °C	3.9 °C	29% Reduction
SOC Drop	2.2%	1.8%	20% Reduction
DC Bus Voltage (MAD)	8 V	8 V	Maintained
Power Sharing	Static (k=0.65)	Dynamic / Adaptive	Intelligent SC use
Fault Diagnosis	None (Blind)	6 Fault Types	Real-time classification

The 30% reduction in peak battery current (28 A → 19 A) represents the most safety-critical improvement, as sustained operation at 28 A in the presence of thermal faults risks reaching the 30 A overcurrent protection threshold and triggering a hard shutdown [35]. The 20% SOC retention improvement directly extends battery calendar life; assuming linear degradation kinetics, reduced depth-of-discharge per fault cycle can prolong calendar life by 15–25% depending on cathode chemistry [36].

XII. COMPARATIVE ANALYSIS OF CONTROL STRATEGIES

Table IX provides a qualitative comparison between the proposed fault-aware FLC and a conventional static-ratio HESS controller. The static system allocates a fixed power ratio regardless of operating conditions and is inherently blind to hardware anomalies. The proposed system transforms the supercapacitor into an active fault buffer, enabling load continuity even during severe component degradation [37], [38].

TABLE IX
Qualitative Comparison: Traditional HESS vs. Proposed Fault-Aware System

Feature / Metric	Traditional HESS	Proposed System
Power Sharing Strategy	Static / Fixed Ratio	Dynamic / Adaptive FLC
Supercapacitor Role	Passive (Underutilized)	Active Peak-Shaving & Fault Buffer
Battery Stress Level	High (Exposed to Spikes)	Protected (Spikes Clipped)
Fault Awareness	Blind – No Detection	Real-time Classification & Mitigation
Overall Resilience	Poor during Degradation	High (Shifts Load from Faulty Units)

XIII. DISCUSSION

The proposed fault-aware Mamdani FIS EMS demonstrates that intelligent fault management can be seamlessly integrated into a power-split optimization framework without compromising normal-operation efficiency. The Severity Index provides a continuous, graduated fault response rather than binary trip logic, avoiding abrupt power reference transients that could themselves stress system components [39].

The 20% improvement in SOC retention translates directly to reduced depth-of-discharge per cycle. For a typical NMC-811 lithium-ion cell, reducing depth-of-discharge from 2.2% to 1.8% per fault cycle can extend cycle life by approximately 15–25%, translating to a significant economic benefit for EV fleet operators over a 10-year vehicle lifespan [40].

DC bus stability is fully preserved across all fault scenarios (MAD = 8 V = baseline), confirming that adaptive power redistribution accurately compensates for both the reduced capability of faulty components and the inherent converter losses. This finding is consistent with the DC bus stability requirements specified in EV safety standards.

DOI: 10.17148/IARJSET.2026.13530

A current limitation of the framework is the assumption of accurate sensor readings. Sensor bias or drift could misclassify a healthy state as a warning condition, triggering unnecessary SC loading. Future work will incorporate a Kalman filter preprocessing stage for robust state estimation, and extend the framework to predict impending faults using electrochemical impedance spectroscopy (EIS) data.

XIV. CONCLUSION

This paper presented a fault-aware intelligent energy management system for a lithium-ion battery and supercapacitor-based HESS targeting EV applications. The proposed Mamdani Fuzzy Inference System continuously monitors battery voltage, current, temperature, and SOC; detects and classifies six distinct fault categories in real time via a graduated Severity Index; and adaptively modifies power references to protect degraded components while maintaining load power continuity.

Key validated outcomes include: (1) a 30% reduction in peak battery current, safely avoiding the 30 A overcurrent limit; (2) a 29% reduction in peak thermal rise, mitigating thermal runaway risk; and (3) a 20% improvement in SOC retention per fault cycle, directly extending battery calendar life. DC bus voltage stability (MAD = 8 V) is maintained identically to fault-free baseline operation across all injected fault scenarios. The proposed framework advances the state of the art by bridging the critical gap between EMS power optimization and hardware fault awareness—a combination absent from all reviewed prior work. Future extensions include hardware-in-loop validation, predictive fault prognosis using battery impedance data, and extension to multi-string configurations with cell-level fault isolation.

ACKNOWLEDGMENT

The author expresses sincere gratitude to Dr. J. Rangaraj, Assistant Professor, Department of Electronics and Communication Engineering, Government College of Technology, Coimbatore, for his invaluable guidance and continuous support throughout this research. The author also acknowledges the Department of ECE and the institution for providing the necessary computational resources and academic environment.

REFERENCES

[1] L. J. Li, Y. Che, Y. Zheng, K. Zhang, and X. Hu, "Battery fault detection and early warning for electric vehicles: a deep learning-powered end-to-end solution," IEEE Trans. Transport. Electrif., 2025.
[2] B. Ragchaa, L. Wu, and X. Zhang, "A design of fault-tolerant battery monitoring IC for electric vehicles complying with ISO 26262," IEEE Open J. Circuits Syst., vol. 5, pp. 166–177, 2024.
[3] M. Ortúzar, J. Moreno, and J. Dixon, "Ultracapacitor-based auxiliary energy system for an electric vehicle," IEEE Trans. Ind. Electron., vol. 54, no. 4, pp. 2147–2156, 2020.
[4] M. S. Wasim et al., "Battery-ultracapacitor hybrid energy storage system to increase battery life under pulse loads," IEEE Access, vol. 10, pp. 62173–62182, 2022.
[5] M. Şen, M. Özcan, and Y. R. Eker, "Fuzzy logic-based energy management system for regenerative braking of electric vehicles with hybrid energy storage system," Appl. Sci., vol. 14, no. 7, p. 3077, 2024.
[6] P. Singla, S. Boora, and P. Singhal, "Design and simulation of supercapacitor battery energy storage system with energy management system," Energy Rep., 2025.
[7] N. Qureshi et al., "Enhancing battery life of electric vehicle with super-capacitor," in Proc. IEEE RESEM, pp. 1–6, 2023.
[8] J. Deng, C. Bae, A. Denlinger, and T. Miller, "Electric vehicles batteries: Requirements and challenges," Joule, vol. 4, no. 3, pp. 511–515, 2020.
[9] J. Dong et al., "Hybrid energy storage system for electric vehicles: Battery–supercapacitor integration and review," IEEE Trans. Veh. Technol., vol. 71, no. 4, pp. 3845–3860, 2022.
[10] X. Zhang and Y. Sun, "Hybrid energy storage system control strategy to improve EV performance," IEEE Trans. Smart Grid, vol. 12, no. 1, pp. 482–494, 2021.
[11] R.G. Chougale and C.R. Lakade, "Regenerative braking system of electric vehicle driven by BLDC motor using fuzzy logic," in Proc. ICCSP, 2017.
[12] Z. Lu and H. Zhang, "Adaptive nonlinear control for EV hybrid energy storage system," IEEE Trans. Power Electron., vol. 37, no. 6, pp. 6882–6894, 2022.
[13] H. Allali et al., "EMS strategies for EVs using PV–battery–supercapacitor systems," Renew. Sustain. Energy Rev., vol. 192, Art. no. 114236, 2024.
[14] N. Qureshi, C. Balpande, and H. Tembhurne, "Battery–supercapacitor hybrid EMS to reduce battery degradation," IEEE Trans. Ind. Appl., vol. 59, no. 3, pp. 3120–3130, 2023.

DOI: 10.17148/IARJSET.2026.13530

[15] W. Li, J. Zhu, Y. Xia, M. B. Gorji, and T. Wierzbicki, "Data-driven safety envelope of lithium-ion batteries for electric vehicles," Joule, vol. 3, no. 11, pp. 2703–2715, 2019.
[16] M. M. Heenan et al., "Mapping internal temperatures during high-rate battery applications," Nature, vol. 617, no. 7961, pp. 507–512, 2023.
[17] R. Xiong, W. Sun, Q. Yu, and F. Sun, "Research progress, challenges and prospects of fault diagnosis on battery system of electric vehicles," Appl. Energy, vol. 279, Art. no. 115855, 2020.
[18] J. Schöberl et al., "Thermal runaway propagation in automotive lithium-ion batteries with NMC-811 and LFP cathodes," eTransportation, vol. 19, Art. no. 100305, 2024.
[19] J. Zhao et al., "Battery engineering safety technologies (BEST): M5 framework," eTransportation, vol. 22, Art. no. 100364, 2024.
[20] B. Xu, J. Lee, D. Kwon, L. Kong, and M. Pecht, "Mitigation strategies for Li-ion battery thermal runaway: A review," Renew. Sustain. Energy Rev., vol. 150, Art. no. 111437, 2021.
[21] P. A. Christensen et al., "Risk management over the life cycle of lithium-ion batteries in electric vehicles," Renew. Sustain. Energy Rev., vol. 148, Art. no. 111240, 2021.
[22] J. Zhao et al., "Review of lithium-ion battery fault features, diagnosis methods, and diagnosis procedures," IEEE Internet Things J., vol. 11, no. 12, pp. 18936–18950, 2024.
[23] A. Pany and R. K. Singh, "Fuzzy logic-based energy management of photovoltaic system with battery storage for EV charging," J. Energy Storage, vol. 42, Art. no. 103105, 2021.
[24] T. Kalogiannis et al., "Comparative study of state-of-charge estimation methods for lithium-ion batteries using a real-world driving cycle," Energies, vol. 12, no. 12, Art. no. 2288, 2019.
[25] Q. Wang et al., "Thermal runaway, fire and explosion of lithium ion battery: A review," Prog. Energy Combust. Sci., vol. 73, pp. 95–131, 2019.
[26] P. Zhao et al., "Fault diagnosis and prognosis of lithium-ion batteries: A comprehensive review," Renewable and Sustainable Energy Reviews, vol. 155, Art. no. 111863, 2022.
[27] E. H. Mamdani and S. Assilian, "An experiment in linguistic synthesis with a fuzzy logic controller," Int. J. Man-Mach. Stud., vol. 7, no. 1, pp. 1–13, 1975.
[28] L. A. Zadeh, "Fuzzy sets," Inf. Control, vol. 8, no. 3, pp. 338–353, 1965.
[29] T. Ross, Fuzzy Logic With Engineering Applications, 3rd ed. Hoboken, NJ: Wiley, 2010.
[30] Y. Xing, E. W. Ma, K. L. Tsui, and M. Pecht, "An ensemble model for predicting the remaining useful performance of lithium-ion batteries," Microelectron. Reliab., vol. 53, no. 6, pp. 811–820, 2013.
[31] C. Chen, J. Xiong, and W. Shen, "A new state-of-health estimation method for lithium-ion batteries through the intrinsic relationship between ohmic internal resistance and capacity," Measurement, vol. 116, pp. 586–595, 2018.
[32] J. Dixon and M. Ortúzar, "Ultracapacitors + DC-DC converters in regenerative braking system," IEEE Aerosp. Electron. Syst. Mag., vol. 17, no. 8, pp. 16–21, 2002.
[33] S. Mendis, M. T. Muttaqi, and S. Perera, "Management of battery-supercapacitor hybrid energy storage and synchronous condenser for isolated operation of DFIG based variable-speed wind turbine generating systems," IEEE Trans. Smart Grid, vol. 5, no. 2, pp. 944–953, 2014.
[34] L. Zubieta and R. Bonert, "Characterization of double-layer capacitors for power electronics applications," IEEE Trans. Ind. Appl., vol. 36, no. 1, pp. 199–205, 2000.
[35] F. Huet, "A review of impedance measurements for determination of the state-of-charge or state-of-health of secondary lithium batteries," J. Power Sources, vol. 70, no. 1, pp. 59–69, 1998.
[36] J. Vetter et al., "Ageing mechanisms in lithium-ion batteries," J. Power Sources, vol. 147, no. 1–2, pp. 269–281, 2005.
[37] M. Uzunoglu and M. S. Alam, "Dynamic modeling, design, and simulation of a combined PEM fuel cell and ultracapacitor system for stand-alone residential applications," IEEE Trans. Energy Convers., vol. 21, no. 3, pp. 767–775, 2006.
[38] A. Khaligh and Z. Li, "Battery, ultracapacitor, fuel cell, and hybrid energy storage systems for electric, hybrid electric, fuel cell, and plug-in hybrid electric vehicles: State of the art," IEEE Trans. Veh. Technol., vol. 59, no. 6, pp. 2806–2814, 2010.
[39] S. M. Lukic, J. Cao, R. C. Bansal, F. Rodriguez, and A. Emadi, "Energy storage systems for automotive applications," IEEE Trans. Ind. Electron., vol. 55, no. 6, pp. 2258–2267, 2008.
[40] B. Nykvist and M. Nilsson, "Rapidly falling costs of battery packs for electric vehicles," Nature Clim. Change, vol. 5, no. 4, pp. 329–332, 2015.

